

Early stage equilibration dynamics in a two-component nuclear system

M. Herman, G. Reffo, and C. Costa

Ente Nazionale Energie Alternative, Divisione di Calcolo, 40138 Bologna, Italy

(Received 7 July 1988)

The two-component exciton model is reformulated to facilitate a solution of the master equation and to express transition rates via quasiparticle state densities calculated in the frame of the shell model. On this basis, flux flow between different substages of the composite nucleus is discussed. This analysis shows strong discrepancies in the strength of various transitions. In particular, particle-hole creation by a hole is found to be rather negligible. New closed form expressions for the transition rates, accounting for the shell gaps, are proposed. Their predictions are compared against microscopic results.

INTRODUCTION

The problem of neutron-proton distinction in the equilibration of the composite nucleus was already addressed in the early stages of preequilibrium model development,^{1,2} receiving little attention however. Even after Betak and Dobes³ and later Kalbach⁴ had formulated and applied the two-component version of the exciton model, one-component approaches have been exclusively used in reaction calculations. This may be related to the fact that, on the one hand, two-component calculations are much more involved, and on the other, the results reported in Refs. 3 and 4 do not present a convincing improvement over the one-component version of the model. Most authors prefer, therefore, to account for the proton-proton distinction by introducing a multiplicative factor in the emission rates.⁵⁻⁹ These factors are obtained in a somewhat arbitrary manner, and often differ from each other.

A consistent derivation of the effective one-component exciton model, from the two component formulation, was given by Gupta.⁹ He has shown that, using a one-component model, transitions inconsistent with the assumption of the two-body nature of the equilibration process are included, and that this can be compensated by modification of the averaged matrix element $|M|^2$ without affecting the cross section and spectra predictions. The result by Gupta provides, to some extent, the justification of the one-component model. It is only valid, however, if the state densities for equivalent proton and neutron configurations are the same. In fact, Gupta takes the equidistant spacings of the single-particle states equal to $g/2$ for both nucleon types.

Use of the one-component model also leads to an unavoidable inconsistency in the state densities for the preequilibrium and the equilibrium part. Actually, the two-gas formula for the state densities, as used in the compound model, is not matched by the one-component expressions of Ericson¹⁰ or of Williams,¹¹ when the latter are summed over all exciton numbers at the equilibrium stage. This deficiency is overcome, naturally, using the two-component formula for the densities of states with a

fixed number of excitons, but this implies use of the two-component model. A compromise solution, followed by several authors,^{12,13} is to normalize the one-component formulae to make them consistent with the predicted state densities in the compound nucleus. These renormalized densities were used in the one-component exciton model,^{12,13,14} showing a significant effect. In general, the results were improved.

Our recent shell-model calculations^{15,16} indicate that the assumption of an equal state density for neutron and proton configurations, underlying the model by Gupta,⁹ usually does not hold. To illustrate this point, in Fig. 1 we present a comparison of the neutron and proton state densities for the two- and four-exciton configurations in ⁹⁰Zr. The calculations were performed following the procedure described in Refs. 15 and 16 using the single-particle states, carefully adjusted to individual nuclei, by Nix and Moller.¹⁷ Figure 1 shows that the thresholds for excitation of the given configurations are clearly different (especially in the four-exciton case), as well as is the structure in the energy distribution of the states. We stress that accounting for these differences is only possible if the explicit two-component formulation of the exciton model is used. This is in contrast to the other, previously mentioned, shortcomings of the one-component model that can be remedied, thus avoiding the necessity of using a more involved two-component version. The latter becomes indispensable when microscopic state densities are used.

In this paper, we follow the approach by Dobes and Betak,³ in writing down the two-component master equation describing equilibration of the composite system. We propose a transformation that facilitates solution of the master equation, and show that this solution exists. For the sake of simplicity we neglect angular momentum and angular distribution considerations. Internal transition and emission rates are expressed in terms of the state densities, allowing for a direct use of the microscopic results. On this basis, the dynamics of the equilibration process is discussed. Finally, microscopically calculated transition rates are compared with the newly proposed closed form expressions, which approximately take into account the shell effects.

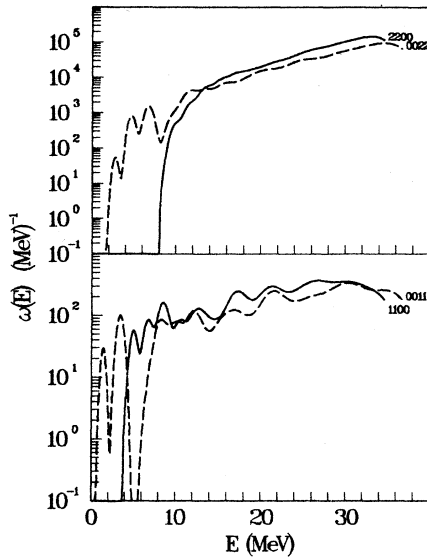


FIG. 1. The densities of two- and four-exciton states for neutrons and protons in ^{90}Zr calculated in the space of the shell-model single-particle states. Different configurations are denoted with $p_v, h_v, p_\pi,$ and h_π .

TWO-COMPONENT EXCITON MODEL

The model is a natural extension of the exciton model to a system of two distinguishable components, as proposed by Dobes and Betak.³ It is based on the same assumptions as the standard exciton model, and we recall here the two-body nature of the residual interaction as the fundamental one. We assume that equilibration of the system may be described in terms of the transitions between the subsequent stages, which are defined according to their complexity. In the exciton model these stages are specified by the number of single-particle degrees of freedom called excitons. The two-body residual interaction implies that the neighboring stages differ by two excitons (one particle and one hole), and that coupling is possible only between neighboring stages. Let us assume that the first stage of the reaction may be described by the target nucleus plus the projectile broken up into its n_0 nucleons. The first stage contains, therefore, no holes but n_0 excitons of particle type. Due to the assumed two-body interaction for each N th stage, two obvious relations hold (we refer to Table I for explanation of the symbols)

$$n = 2(N - 1) + n_0, \quad (1)$$

and

$$h = N - 1, \quad (2)$$

which show that, in the one-component model, N is sufficient to specify the state and that the equilibration proceeds through a one-dimensional chain of stages. When distinguishing between neutrons and protons, we

have to deal formally with five variables: $N, p_v, h_v, p_\pi,$ and h_π . The two-body nature of the interaction implies again several constraints

$$p_v + h_v + p_\pi + h_\pi = 2(N - 1) + n_0, \quad (3)$$

$$h_v = p_v - p_{v0}, \quad (4)$$

$$h_\pi = p_\pi - p_{\pi0}, \quad (5)$$

which reduce the specification of the state to two quantities. Following Gupta,⁹ our choice is to use the reaction stage number N and the number of proton holes h_π . It is important to note that, while for N only the condition $N > 0$ holds, the values of h_π are limited by Eqs. (3), (4), and (5) to $0 \leq h_\pi < N$. Accordingly, each stage N splits into N substages depending on the number of proton holes contained. Using this representation the equilibration of the composite nucleus can be depicted by a two-dimensional plot, as shown in Fig. 2 for the case of a neutron projectile. In the figure, nuclear substages are denoted explicitly by four numbers referring to $p_v, h_v, p_\pi,$ and h_π . Transitions between substages are represented by the arrows labeled with the types of nucleons that are involved in the transition. Coupling of the substages to the decay channels is not shown in the graph.

All transitions in Fig. 2 may be grouped into three categories as follows.

Interstage transitions are characterized by $\Delta N = \pm 1$ and represented on the graph by the diagonal arrows.

Intersubstage transitions are characterized by $\Delta N = 0$ and $\Delta h_\pi = \pm 1$ and represented by the horizontal arrows.

Rearrangement transitions are characterized by $\Delta N = 0$ and $\Delta h_\pi = 0$ and represented by the semi-circle arrows.

The interstage transitions are crucial for the description of the equilibration process. In general, each of them may be realized via the interaction of unlike and one type of the like nucleons. The type of the like nu-

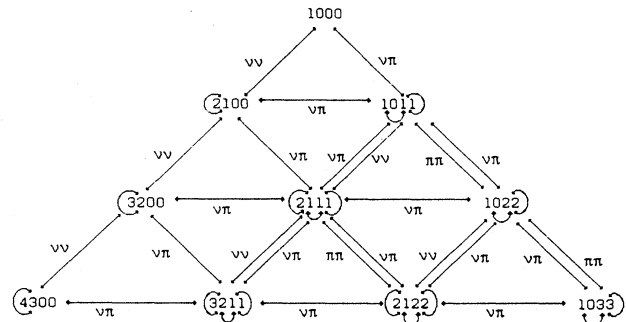


FIG. 2. Schematic diagram of the equilibration of the composite nucleus formed in the neutron induced reaction. Different substages are denoted with $p_v, h_v, p_\pi,$ and h_π . The arrows show the internal transitions consistent with the two-body assumption for the nuclear forces, and are labeled with the type of the interacting nucleons.

cleons depends on the change in the number of proton holes and we have ν - ν interactions for $\Delta h_\pi = 0$ and π - π or ν - π interactions for $\Delta h_\pi = +1$. In practice, it may happen at the edge of the net, that some of these transitions are excluded by the lack of the proper excitons in the substage undergoing a transition (see Fig. 2). Distinction between like and unlike interactions is natural in the two-component model and, differently to the one-component model, allows for taking into account the possible difference in the strength between these two. In free nucleon scattering the latter is known to be approximately three times stronger than the former one. There are, however, some doubts whether the same factor should be applied to the intrinsic interactions in a real nucleus,⁴ and we consider this problem open. In the two-component model also ν - ν and π - π interactions may be further differentiated.

The intersubstage transitions correspond to the part of the $\Delta n = 0$ transitions in the one-component model, and are disregarded therein when the angular distribution is not taken into account. In our case the intersubstage

transitions have to be considered, because they do not cancel in the master equation, due to the additional index h_π . Physically, they describe the redistribution of the excitation energy between neutrons and protons within the same stage, with consequent modification of the population probability for the different substages. The interaction causing the intersubstage transitions is obviously of unlike type, and therefore may be relatively strong.

The rearrangement transitions describe the redistribution of energy between the excitons without any change of the neutron and proton exciton numbers. These interactions may be of like as well as unlike type, and lead to the displacement of two excitons. They do not influence, however, the population probability of the substage, and cancel in the master equation, similarly to the $\Delta n = 0$ transitions in one-component model. The rearrangement transitions would have to be considered if the angular distribution were taken into account.

Using Fig. 2 the master equation describing equilibration of the two-component system is written in the form (see Table I for explanation of the symbols)

TABLE I. Definition of symbols.

ν, π	Subscripts denoting neutrons or protons.
β	Subscript denoting emitted particle.
p, h	Used as a subscript relate a quantity to particle or hole degrees of freedom, respectively.
0	Used as a subscript relates exciton numbers to the initial configuration ($N = 1$).
E	Excitation energy of the composite nucleus.
U	Excitation energy of the residual nucleus.
g	Single particle state density.
p	Number of particle excitons.
h	Number of hole excitons.
n	Total number of excitons.
N	Stage of the reaction.
j	Running index enumerating substages.
$P(N, h_\pi, t)$	Population probability of the substage denoted by N and h_π at time t .
$P(t)$	Population probability vector [components being $P(j, t)$] at time t .
τ	Vector of the average lifetime of the substages [integral of $P(t)$].
A	Matrix of transition and emission rates in the master equation.
$\omega(E, p_\nu, h_\nu, p_\pi, h_\pi)$	Density of states with specified exciton numbers at excitation energy E .
${}^i\omega_{\mu\mu'}^{**}(E, p, h, p, h)$	Density of accessible states (transition density) for the substage specified with the exciton numbers at energy E . The first superscript denotes the change in N (+ for $\Delta N = 1$, 0 for $\Delta N = 0$, and - for $\Delta N = -1$). Similarly, the second superscript denotes the change in h_π . Superscript on the left indicates a diagram (see Fig. 4) to which transition density is related. Lack of any of those superscripts means that the summation over it has been performed. Two subscripts denote type of the nucleons that are involved in the transition.
$ M $	Average transition matrix element.
$w_\beta(\epsilon, N, h_\pi)$	Emission rate of a particle β into the continuum with channel energy ϵ from the configuration denoted by N and h_π .
$W(E, N, h_\pi)$	Total emission of particles into the continuum from the configuration denoted by N and h_π at energy E .
σ_α	Reaction cross section.
σ_β	Inverse cross section.
s_β	Spin of emitted particle.
μ_β	Reduced mass of emitted particle.

$$\begin{aligned}
\frac{d\mathbf{P}(N, h_\pi, t)}{dt} = & [\lambda_{v\pi^+}^{++}(E, N-1, h_\pi-1) + \lambda_{\pi\pi^+}^{++}(E, N-1, h_\pi-1)]\mathbf{P}(N-1, h_\pi-1, t) \\
& + [\lambda_{v\pi^0}^{+0}(E, N-1, h_\pi) + \lambda_{v\pi^0}^{+0}(E, N-1, h_\pi)]\mathbf{P}(N-1, h_\pi, t) \\
& + [\lambda_{v\pi^-}^{-0}(E, N+1, h_\pi) + \lambda_{\pi\pi^-}^{-0}(E, N+1, h_\pi)]\mathbf{P}(N+1, h_\pi, t) \\
& + [\lambda_{\pi\pi^-}^{--}(E, N+1, h_\pi+1) + \lambda_{v\pi^-}^{--}(E, N+1, h_\pi+1)]\mathbf{P}(N+1, h_\pi+1, t) \\
& + \lambda_{v\pi^+}^{0+}(E, N, h_\pi-1)\mathbf{P}(N, h_\pi-1, t) + \lambda_{\pi\pi^+}^{0+}(E, N, h_\pi+1)\mathbf{P}(N, h_\pi+1, t) \\
& - [\lambda_{v\pi^0}^{+0}(E, N, h_\pi) + \lambda_{\pi\pi^0}^{+0}(E, N, h_\pi) + \lambda_{v\pi^+}^{++}(E, N, h_\pi) + \lambda_{\pi\pi^+}^{++}(E, N, h_\pi) \\
& + \lambda_{v\pi^-}^{-0}(E, N, h_\pi) + \lambda_{\pi\pi^-}^{-0}(E, N, h_\pi) + \lambda_{v\pi^0}^{-0}(E, N, h_\pi) + \lambda_{v\pi^0}^{-0}(E, N, h_\pi) \\
& + \lambda_{\pi\pi^0}^{-0}(E, N, h_\pi) + \lambda_{v\pi^+}^{0+}(E, N, h_\pi) + W(E, N, h_\pi)]\mathbf{P}(N, h_\pi, t) .
\end{aligned} \tag{6}$$

The internal transition rates λ will be defined and discussed further on in Sec. II. The emission rates $W(E, N, h_\pi)$ are written in analogy to the one-component exciton model, having one-gas state densities replaced by the two-gas quantities

$$\begin{aligned}
W_\beta(\varepsilon, N, h_\pi) = & \frac{2s_\beta + 1}{\pi^2 \hbar^3} \mu_\beta \varepsilon \sigma_\beta(\varepsilon) \\
& \times \frac{\omega(E - \varepsilon, p_v - p_{v\beta}, h_v, p_\pi - p_{\pi\beta}, h_\pi)}{\omega(E, p_v, h_v, p_\pi, h_\pi)} ,
\end{aligned} \tag{7a}$$

$$W(N, h_\pi) = \sum_\beta \int W_\beta(\varepsilon, N, h_\pi) d\varepsilon . \tag{7b}$$

We again refer to Table I for the definition of the symbols. Terms corresponding to the emission from the substages not containing the proper type of particle excitons have to vanish in Eq. (7).

In comparison with the one-component model, which is described by a three diagonal matrix, the two-component master equation appears to be appreciably more complicated, even though linear and angular momenta were neglected. We have to deal not only with seven terms instead of three but, first of all, the population probability is a two-dimensional matrix instead of a vector. To facilitate the solution of the master equation we transform the two-dimensional population matrix into a vector. We note, that because of $h_\pi < N$, the population matrix in Eq. (6) is in fact triangular. Accordingly, we can ascribe a running index “ j ” to each substage starting from the top of Fig. 2 and enumerating along subsequent rows from the left to the right. The new index “ j ” is related to N and h_π by a simple relation

$$j = N(N-1)/2 + h_\pi + 1 , \tag{8}$$

and it is sufficient to specify a substage completely, because N and h_π may be obtained for each “ j ” through the expressions

$$N = \text{INT}(0.5 + \sqrt{2j - 1.75}) \tag{9}$$

and

$$h_\pi = j - N(N-1)/2 - 1 , \tag{10}$$

where INT stands for the Entier function. This way, the Eq. (6) has been transformed into the standard system of linear differential equations. To specify it, we have to write the matrix in Eq. (6) in terms of “ j .” Let us note, that in the (N, h_π) representation the following “selection rules” for the internal transitions hold

$$\begin{aligned}
\Delta N = -1; \Delta h_\pi = -1, 0 , \\
\Delta N = 0; \Delta h_\pi = 1, -1 , \\
\Delta N = 1; \Delta h_\pi = 0, 1 ,
\end{aligned}$$

with boundary conditions $N > 0$ and $0 \leq h_\pi < N$. Transforming these selection rules to the j representation, it is easy to show that a given substage j is coupled to the following i substages.

$i = j - N + 1$ and $i = j - N$ through $\Delta N = -1$ transitions with boundary condition $(N-2)(N-1)/2 < i \leq N(N-1)/2$.

$i = j + 1$ and $i = j - 1$ through $\Delta N = 0$ transitions with the boundary condition $N(N-1)/2 < i \leq N(N+1)/2$.

$i = j + N$ and $i = j + N + 1$ through the $\Delta N = 1$ transitions with no boundary condition.

For the convenience of the notation we still make use of N , even though it could be avoided employing Eq. (9). The master equation rewritten using index j may seem to have a strange structure, and the boundary conditions become more complicated than in the (N, h_π) representation. In Fig. 3 we show, however, that the two-component master equation indexed with j nicely links to the one-component version. To elucidate this feature, the thick horizontal and vertical lines are drawn to separate the reaction stages. Clearly, master equation matrix remains tridiagonal in the N representation, which corresponds to the one-component model. The appropriate one-component transition rates can be obtained by summing the two-component transition rates over the second superscript (whole blocks in Fig. 3) to give λ^- , λ^0 and λ^+ . In the two-component model each N th stage is split into N substages, and two diagonals are filled in each block corresponding to the $\Delta N = \pm 1$ transitions, and three diagonals in the case of $\Delta N = 0$. The boundary conditions represent a trivial restriction that all transitions have to be contained in the three neighboring blocks. Figure 3 also shows the shortcomings of the one-component model, which assumes that all substages of a

N	j									
	1	2	3	4	5	6	7	8	9	10
1	1	L	λ^{-0}	λ^{-}						
	2	λ^{+0}	L	λ^{0-}	λ^{-0}	λ^{-}				
2	3	λ^{++}	λ^{0+}	L		λ^{-0}	λ^{-}			
	4		λ^{+0}		L	λ^{0-}		λ^{-0}	λ^{-}	
3	5		λ^{++}	λ^{0+}	λ^{0+}	L	λ^{0-}		λ^{-0}	λ^{-}
	6			λ^{++}		λ^{0+}	L			λ^{-0}
	7				λ^{+0}			L	λ^{0-}	
4	8				λ^{++}	λ^{0+}		λ^{0+}	L	λ^{0-}
	9					λ^{++}	λ^{0+}		λ^{0+}	L
	10						λ^{++}			L

FIG. 3. Schematic representation of the j -indexed master equation. Thick lines separate different stages of the equilibration process. Off-diagonal elements represent gain of the flux from other substages, while diagonal elements L are responsible for the loss of the flux due to the coupling to other substages and to the open channels.

given stage are coupled to all substages of the next stage. This assumption fails at the second step of the equilibration chain, because not all substages of $N=3$ can be reached from both substages of $N=2$. Those unavailable are represented by empty squares in Fig. 3. With increasing N , blocks become more and more "empty" indicating increasing role of the proton-proton distinction.

Following the method of Luider¹⁸ it is easy to show that the solution of Eq. (6) exists. Let A be the matrix formed by the transition and emission rates in the master equation. The sum over all elements of each i th column of A gives the emission from the i th substage, since all internal transitions cancel out. Because the emission is always negative,¹⁹ the matrix A is negative diagonal dominant, and the Gerschgorin theorem²⁰ applies. It follows that all eigenvalues of A are nonzero, real and negative. This general feature of all matrices describing the equilibration of any system via internal transitions and emission was pointed out by Luider.²¹ Here, we show that the A matrix in our j representation also bears these characteristics. Using $P(t)$ for the population probability vector, we can rewrite Eq. (6) in the matrix form

$$\dot{P}(t) = AP(t). \quad (11)$$

The formal solution of Eq. (11) reads

$$P(t) = \exp(At)P(0). \quad (12)$$

In most of the applications, we are interested in the time integral of $P(t)$, which gives average lifetimes τ of the substages. Because all eigenvalues of A are nonvanishing, real, and negative, Eq. (12) can be integrated from zero to infinity to give

$$A\tau = -P(0). \quad (13)$$

Similar to the one-component model, we have to solve a set of linear equations. This set is appreciably larger, and more complicated (as A is no longer tridiagonal) than in the one-component case but, due to the negative diagonal dominance, a unique solution exists, and can be obtained using standard numerical procedures.

The differential cross section is given finally by

$$\frac{d\sigma_{\alpha\beta}(\epsilon)}{d\epsilon} = \sigma_{\alpha} \sum_j W_{\beta}(\epsilon, j) \tau(j). \quad (14)$$

INTERNAL TRANSITION RATES

Assuming two-body interaction, there are 18 diagrams that contribute to internal transitions. Figure 4 shows how particular transition rates are constructed. Following the standard procedure based on Fermi's golden rule, a transition rate λ may be written in general as

$$\lambda = \frac{2\pi}{\hbar} |M|^2 \omega_f, \quad (15)$$

where the average squared matrix element $|M|^2$ is, as usual, a parameter of the model, and ω_f stands for the density of final accessible states. In the two-component formulation one can distinguish between the $|M|^2$ corresponding to neutron-neutron, proton-proton, and proton-neutron interaction. In practice, it is presumably sufficient to deal with two matrix elements, one for like and one for unlike interactions.

To calculate the density of accessible states, entering Eq. (15), we assume equal population probability for all configurations in a given substage. The system is split into the interacting part, which contains the excitons taking part in the interaction, and the passive part that behaves like a spectator. The probability of finding the required interacting part with energy ϵ , is given, according to our assumption, by the ratio of the state density of the passive part at energy $E-\epsilon$ to the density of states for the whole system at energy E . The total number of interacting configurations is obtained as a product of the above probability and the density of states for the interacting part. To obtain the density of accessible states, we multiply the above with the density of the interacting part in the final state and integrate over ϵ from 0 to E . This simple procedure requires performing one numerical integration if the state densities are given in a tabulated form, whereas analytical expressions are straightforward if state densities are given in terms of the energy polynomials (such as the formulas of Ericson and of Williams). For example, the density of accessible states associated with the third diagram reads

$${}^3\omega_{\nu\pi}^{++}(E) = \int_0^E d\epsilon \frac{\omega(E-\epsilon, p_{\nu}-1, h_{\nu}, p_{\pi}, h_{\pi})}{\omega(E, p_{\nu}, h_{\nu}, p_{\pi}, h_{\pi})} \times \omega(\epsilon, 1, 0, 0, 0) \omega(\epsilon, 1, 0, 1, 1). \quad (16)$$

Similar expressions for the remaining 17 diagrams are easily obtainable applying the above procedure.

The transition rates are obtained by applying the golden rule [Eq. (15)] and summing the appropriate diagrams of Fig. 4. In the case of λ^{++} we get, for example,

$$\lambda^{++} = \frac{2\pi}{\hbar} (M_{\pi\pi}^2 \omega + M_{\pi\nu}^2 \omega + M_{\nu\nu}^2 \omega + M_{\nu\pi}^2 \omega). \quad (17)$$

In Eq. (16) the Pauli principle is only included in the state densities. Some error still remains due to the fact that the interacting and spectator parts are treated separately. Both of the densities which concern the interacting part are, therefore, overestimated since the single-particle states occupied in the passive part should be made unavailable. The error connected with the partial neglect of the Pauli principle is expected to be rather small, because the model will be used principally for the very early stages of the reaction, where the exciton number is low, and because the neutron-proton distinction decreases the effect of the Pauli principle.

PAIRING CORRECTION

Methods for the correction of the state densities for the pairing interaction were recently proposed by Fu²³ and in

our previous papers.^{15,16} Both methods consist in shifting state distribution by an appropriate pairing energy. The introduction of these corrections into the expressions for the accessible state densities is, however, not straightforward. The difficulty arises, because in the context of the pairing interaction, splitting of the system into active and passive part is not easy to treat. In fact, pairing corrections, calculated for passive and active parts as taken apart, are not appropriate. Actually, BCS equations have to be solved for the entire system, accounting for all excitons the block single particle levels. This would lead to combinatorial calculations of accessible state densities, so complicated and lengthy, to be impractical. We propose, instead, to use pairing corrections (see Refs. 15 and 16) as determined for the entire decaying configuration (P_i) and for the final one (P_f), and apply these shifts to the state densities in Eq. (16). Accordingly, all state densities related to the configuration before the transition should be shifted by P_i , and those related to final

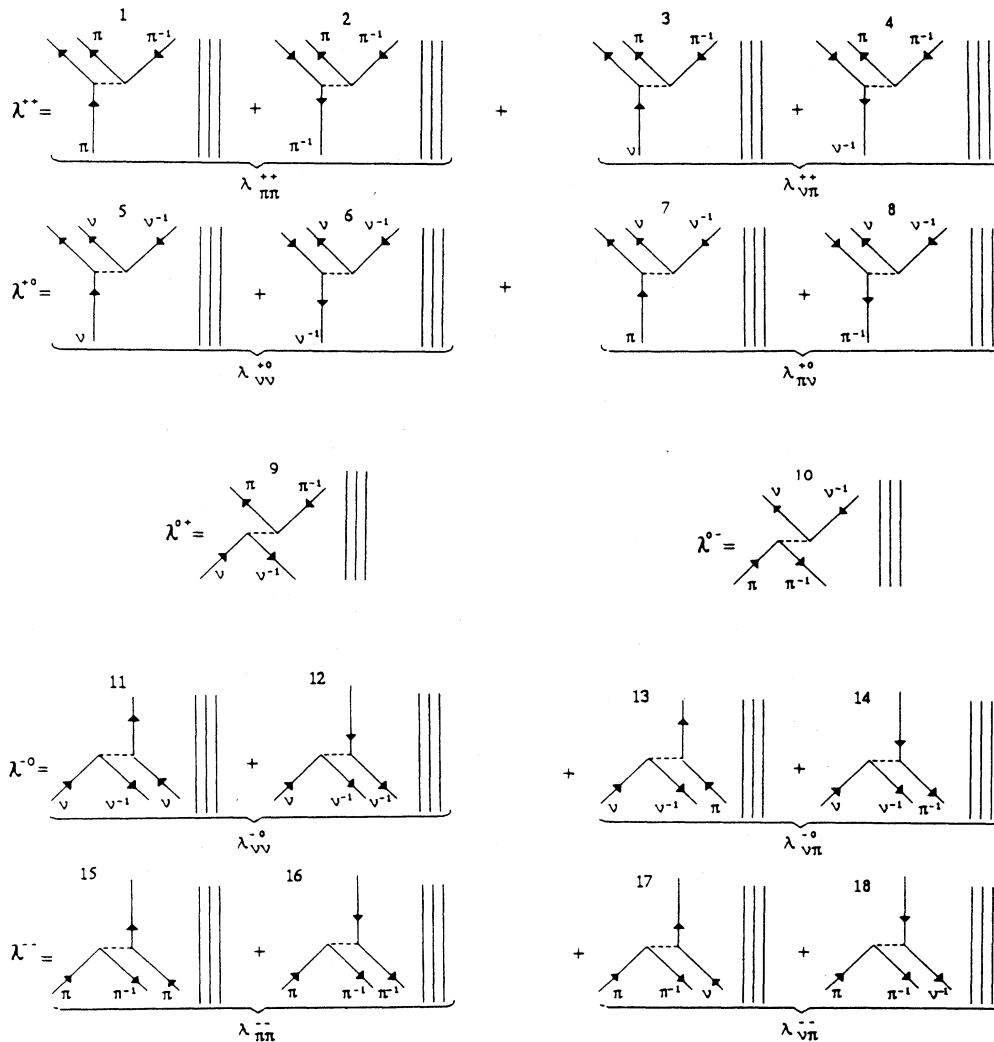


FIG. 4. Diagrams illustrating internuclear transitions in the two-component exciton model. Interacting particles (holes) are represented by upward (downward) arrows, and their nucleon type is indicated. Vertical lines stand for the passive excitons. The diagrams are enumerated to facilitate reference.

configuration by P_f . We give no estimate for the accuracy of the above procedure, but in view of the discussion in Ref. 15, it seems to be reasonable.

In the following section we neglect pairing interaction, which we assume to not have a strong impact on our further discussion.

CLOSED FORM EXPRESSIONS FOR ACCESSIBLE STATE DENSITY

The analytical expressions for the accessible state densities are obtained using the two-component formula for state densities²⁴

$$\omega(E, p_v, h_v, p_\pi, h_\pi) = \frac{g_{p_v}^{p_v} g_{h_v}^{h_v} g_{p_\pi}^{p_\pi} g_{h_\pi}^{h_\pi} (E - S_T)^{n-1}}{p_v! h_v! p_\pi! h_\pi! (n-1)!} \theta(E - T). \quad (18)$$

For reasons which will become clear later, we differentiate between single-particle state densities for particles and holes (g_p and g_h , respectively). Energy shift S_T contains the Pauli correction and, if necessary, pairing shift P . In Eq. (18) we include also Heaviside function $\theta(E - T)$, which excludes states below the threshold T for a given exciton configuration. This way, the most important effect of the shell structure is taken into account.

Using Eq. (18) expressions analogous to Eq. 16 can be integrated analytically. For the accessible state densities corresponding to the first eight diagrams of Fig. 4, one obtains

$${}^1\omega_{\pi\pi}^{++}(E) = \frac{P_\pi g_{p_\pi}^2 g_{h_\pi}}{4(E - S_T)n - 1} F(E, n), \quad (19a)$$

$${}^2\omega_{\pi\pi}^{++}(E) = \frac{h_v g_{h_v}^2 g_{p_\pi}}{4(E - S_T)n - 1} F(E, n), \quad (19b)$$

$${}^3\omega_{v\pi}^{++}(E) = \frac{P_v g_{p_v} g_{h_\pi} g_{p_\pi}}{2(E - S_T)^{n-1}} F(E, n), \quad (19c)$$

$${}^4\omega_{v\pi}^{++}(E) = \frac{h_v g_{h_v} g_{p_\pi} g_{h_\pi}}{2(E - S_T)^{n-1}} F(E, n), \quad (19d)$$

$${}^5\omega_{v\nu}^{+0}(E) = \frac{P_v g_{p_v}^2 g_{h_v}}{4(E - S_T)^{n-1}} F(E, n), \quad (19e)$$

$${}^6\omega_{v\nu}^{+0}(E) = \frac{h_v g_{h_v}^2 g_{p_v}}{4(E - S_T)^{n-1}} F(E, n), \quad (19f)$$

$${}^7\omega_{v\pi}^{+0}(E) = \frac{P_\pi g_{p_\pi} g_{h_\pi} g_{p_v}}{2(E - S_T)^{n-1}} F(E, n), \quad (19g)$$

$${}^8\omega_{v\pi}^{+0}(E) = \frac{h_\pi g_{h_\pi} g_{h_v} g_{p_v}}{2(E - S_T)^{n-1}} F(E, n), \quad (19h)$$

where

$$F(E, n) = a^{n-1} \left[c_2^2 + \frac{2ac_3}{n} + \frac{2a^2}{n(n+1)} \right] - b^{n-1} \left[d_3^2 + \frac{2bd_3}{n} + \frac{2b^2}{n(n+1)} \right].$$

For the intersubstage transitions corresponding expressions read

$${}^9\omega_{v\pi}^{0+}(E) = \frac{P_v h_v (n-1) g_{p_\pi} g_{h_\pi}}{(E - S_T)^{n-1}} G(E, n), \quad (20a)$$

$${}^{10}\omega_{v\pi}^{0-}(E) = \frac{P_\pi h_\pi (n-1) g_{p_v} g_{h_v}}{(E - S_T)^{n-1}} G(E, n), \quad (20b)$$

where

$$G = a^{n-2} \left[T^2 + TS + S_2 S_3 + \frac{a}{n-1} \left[2T + \frac{2a}{n} + S \right] \right] - b^{n-2} \left[e^2 + eS + S_2 S_3 + \frac{b}{n-1} \left[2e + \frac{2b}{n} + S \right] \right].$$

For the remaining backward transitions from substages with $n > 3$ we have

$${}^{11}\omega_{v\nu}^{-0}(E) = \frac{P_v h_v (p_v - 1)(n-2)(n-1) g_{p_v}}{4(E - S_T)^{n-1}} H(E, n), \quad (21a)$$

$${}^{12}\omega_{v\nu}^{-0}(E) = \frac{P_v h_v (h_v - 1)(n-2)(n-1) g_{h_v}}{4(E - S_T)^{n-1}} H(E, n), \quad (21b)$$

$${}^{13}\omega_{v\pi}^{-0}(E) = \frac{P_v h_v p_\pi (n-2)(n-1) g_{p_\pi}}{2(E - S_T)^{n-1}} H(E, n), \quad (21c)$$

$${}^{14}\omega_{v\pi}^{-0}(E) = \frac{P_v h_v h_\pi (n-2)(n-1) g_{h_\pi}}{2(E - S_T)^{n-1}} H(E, n), \quad (21d)$$

$${}^{15}\omega_{\pi\pi}^{--}(E) = \frac{P_\pi h_\pi (p_\pi - 1)(n-2)(n-1) g_{p_\pi}}{4(E - S_T)^{n-1}} H(E, n), \quad (21e)$$

$${}^{16}\omega_{\pi\pi}^{--}(E) = \frac{P_\pi h_\pi (h_\pi - 1)(n-2)(n-1) g_{h_\pi}}{4(E - S_T)^{n-1}} H(E, n), \quad (21f)$$

$${}^{17}\omega_{\pi\nu}^{--}(E) = \frac{P_\pi h_\pi p_\nu (n-2)(n-1) g_{p_\nu}}{2(E - S_T)^{n-1}} H(E, n), \quad (21g)$$

$${}^{18}\omega_{\pi\nu}^{--}(E) = \frac{P_\pi h_\pi h_\nu (n-2)(n-1) g_{h_\nu}}{2(E - S_T)^{n-1}} H(E, n), \quad (21h)$$

where

$$H = a^{n-3} \left[c_2^2 + \frac{2ac_2}{n-2} + \frac{2a^2}{(n-1)(n-2)} \right] - b^{n-3} \left[d_2^2 + \frac{2bd_2}{n-2} + \frac{2b^2}{(n-2)(n-1)} \right].$$

For the substages with $n = 3$ backward transition densities are given by the single particle state densities ap-

appropriate for an active exciton in the final configuration. In Eqs. (19), (20), and (21) the following substitutions were used

$$T = \max(T_2, T_3),$$

$$S = S_2 + S_3,$$

$$a = E - S_1 - T,$$

$$b = T_1 - S_1,$$

$$c_i = T - S_i,$$

$$d_i = E - T_1 - S_i,$$

$$e = E - T_1.$$

Here, T_i is a configuration threshold and subscript i indicates that T or S is related to the passive part of the configuration ($i=1$), active part before a transition ($i=2$), or active part after a transition ($i=3$). Obviously, each T_i is supposed to be greater than S_i , and Eqs. (19), (20), and (21) have meaning only for energies $E > T_1 + T_2$. Below this energy, transitions are not possible and the corresponding accessible state density must vanish.

The complicated structure of Eqs. (19), (20), and (21) is the price we have to pay for including the shell gap and Pauli correction in closed formulas. If thresholds T and pairing shifts are set to zero, and g for particles and holes are taken equal, these formulas essentially reduce to the expressions obtained in Ref. 4. The only minor difference regards the treatment of the Pauli correction. For example, the sum of our Eqs. (19c) and (19d) contains in nominator the correction term $A(p_\pi, h_\pi, p_\nu - 1, h_\nu)$ instead of the $A(p_\pi + 1, h_\pi + 1, p_\nu, h_\nu)$ as found in Eq. (11) of Ref. 4. Proceeding further, and setting Pauli correction to zero, taking all g equal, and disregarding the difference between like and unlike transition strengths still simpler expressions for λ reported by Gupta⁹ are recovered.

EQUILIBRATION OF A COMPOSITE NUCLEUS

Flux flow through particular substages of the composite system may be qualitatively discussed on the basis of the transition rates, without solving master equation. Assuming all matrix elements equal, discussion can be carried out in terms of the accessible densities. We choose the latter, because of the unresolved controversy concerning relative strength of the like and unlike interactions,⁴ and because a value of $|M|^2$ consistent with the new state densities has not yet been determined.

Accessible state densities were obtained, performing numerical integration of Eq. (16), in which microscopically calculated state densities were used. Microscopic calculations were performed according to the method described in Refs. 15 and 16 in the space of the shell-model orbitals as determined by Nix and Möller.¹⁷ No explicit interactions between particles was assumed. To simulate natural level width and configuration mixing, the Gaussian strength distribution was ascribed to each nuclear state. This results in smoothing the calculated state densities, which otherwise show unphysical fluctuations

stemming from representation of nuclear states by sharp lines of zero width. The particular choice of the Gaussian should not be very critical with respect to other possibilities (e.g., Breit-Wigner). The final result depends mostly on the width of the distribution which has been taken of the order of the spreading width of the corresponding configuration.

To demonstrate clearly the effects of the shell structure, we choose ⁹⁰Zr, which is a magic nucleus in respect to neutrons while protons fill roughly half of the shell. Let us concentrate on the (2100) and (1011) configurations, which are the initial configurations of the composite nucleus formed after a neutron absorption by ⁸⁹Zr. These two are also most important as far as the preequilibrium emission is concerned. In Fig. 5 several representative accessible state densities, associated with the appropriate decay processes (see Fig. 4) of both configurations are shown.

In the decay of (2100) configuration, creation of the proton particle-hole pair by a neutron particle (diagram 3 of Fig. 4) is a leading process. Creation of the neutron particle-hole pair (diagram 5) becomes only important above 20 MeV of excitation energy and is by factor of 2 less probable. This difference would further increase if the unlike transitions were favored over the like ones. We note, that analogous transition caused by the neutron hole (diagram 6) is an order of magnitude weaker. We shall return to this point later on. The intersubstage transitions are realized via diagram 9, corresponding to the annihilation of the neutron particle-hole pair and subsequent creation of the proton one. Accessible state density for this process is found to be approximately 10 times lower than for the leading (exciton creating) diagrams. For the backward transitions (diagram 11) the same ratio

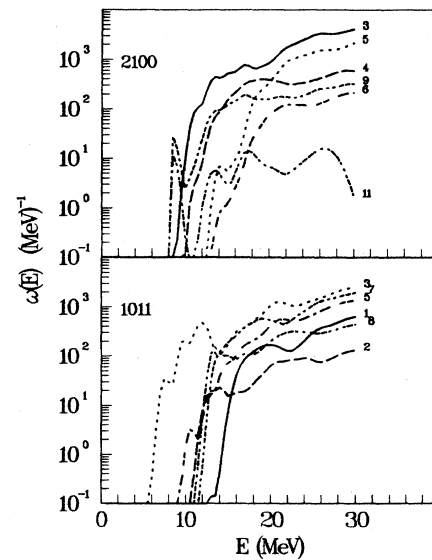


FIG. 5. Accessible state densities for the decay of (2100) and (1011) substages in ⁹⁰Zr as a function of excitation energy. Curves are denoted by numbers, which relate them to the appropriate diagrams of Fig. 4. Calculations were performed in the space of single particle states as determined by Nix and Moeller (Ref. 17).

exceeds 100.

In the case of the (1011) configuration there are more decay possibilities, since both types of nucleon can induce a transition. In Fig. 5 we show, therefore, only most important ones, that correspond to the creation of an exciton pair. Below 12 MeV of excitation energy of the configuration decays nearly exclusively via the proton pair creation induced by the neutron particle (diagram 3). Above this energy, also other decay modes become possible. Accessible state densities for these transitions differ from each other by up to an order of magnitude, and one notes that those induced by holes (diagram 2 and 8) are even lower.

In both cases strongest effect of the shell structure is observed at low excitation energies. Similar to state densities also accessible state densities reveal thresholds, that are scattered over a broad energy range (between 4 and 14 MeV in the case of 1011 configuration decay in ^{90}Zr). In this low energy region, one may thus expect strongly nonuniform flow of the flux through different substages. Actually, decay may be dominated by one particular transition mode, as is the case for the 1011 configuration decay. In general, this observation is not very relevant, because of the negligible precompound emission from such low excited states. In the typical region of the pre-equilibrium emission (usually above 16 MeV of excitation energy) all internal decay processes are possible but their relative importance still may differ by an order of magnitude, leading again to nonuniform flow of the flux. In general, due to the Pauli principle accessible state densities for the unlike transitions are higher than those for the like ones. This can be also deduced from the closed formulas Eqs. (19), (20), and (21) noting that either factor 2 or 4 appears in the denominator, depending on the transition type. Therefore, one expects that in any way formed composite system will proceed to its equilibrium containing equal number of proton and neutron degrees of freedom, and that the main part of the flux will pass through the substages lying in the middle of the graph shown in Fig. 2.

Let us now discuss the flow of the flux through various substages during the equilibration of the ^{90}Zr excited to 18.5 MeV as a result of the neutron absorption. We will take into account only forward transitions, since neglect of the backward and $\Delta N = 0$ transitions is fully justified for the first stages of the equilibration chain. Particle emission, also, is not supposed to affect the results of our discussion. The initial configuration (1000) may decay to (2100) and to (1011) substages. Assuming the decay proportional to the state densities in the appropriate substage we find that 33% of the flux will go to the (2100) substage, while the population of the (1011) substage will be twice as high (67%). We stress again, that this result is solely due to the state densities, since we have assumed equal strength for like and unlike interactions. In the next stage, $N = 3$, we have to consider three substages, namely: (3200), (2111), and (1022). The (2100) substage will decay predominantly to the (2111) substage (83%), and only with 17% to the (3200). The second $N = 2$ substage (1011) will populate (2111) and (1022) nearly equally (53% and 47%, respectively). Thus, we expect following

partition of the flux between three substages with $N = 3$: 6% for (3200), 63% for (2111), and 31% for (1022). This confirms our predictions of nonuniform population probability for the different substages of a given reaction stage. In this particular case, we may expect enhanced proton emission compared to the predictions of the one-component model.

DISCUSSION OF THE CLOSED FORM APPROXIMATION TO STATE DENSITY

Application of the microscopic calculations reported in the previous section is limited to very few initial stages of the reaction, since their complexity increases rapidly with increasing exciton number. On the other hand, the state densities for higher exciton numbers become relatively smooth, and may well be approximated by the Ericson-Williams type expressions. The only important effect of the shell structure is the existence of the threshold energies for excitation of given configurations. This effect has been therefore included in Eqs. (19), (20), and (21). In the following, we verify these expressions comparing them with the microscopic calculations. To this end, configuration threshold energies, that enter Eqs. (19), (20) and (21) were obtained in the microscopic calculations (without smoothing), and value of the single particle state densities $g_{p\nu} = g_{h\nu}$ and $g_{p\pi} = g_{h\pi}$ were taken $N/13$ and $Z/13$, respectively. The comparison of the accessible states densities associated with the decay of 1011 configuration in ^{90}Zr is presented in Figs. 6 and 7. Apparent discrepancy between the predictions of Eqs. (19), (20), and (21), in which configuration thresholds were disregarded (dashed lines), and results of the microscopic calculations (solid lines) is observed. Obviously, it is most dramatic below thresholds. For higher energies closed formulas overestimate microscopic calculations roughly by a factor of 2. Introduction of the configuration thresholds to Eqs. (19), (20), and (21) (dotted lines) clearly improves their performance. First of all, the thresholds are approximately reproduced and in addition the accessible state densities are decreased, that leads to a better agreement with the microscopic results. This reduction is related to the restricted integration interval in Eq. (16), and is most pronounced at excitation energies close to the threshold. Thus, relative importance of the shell gaps decreases with the increasing energy.

The strongest discrepancies between microscopic calculations and closed formulas are observed for the accessible state densities corresponding to the second and eighth diagrams. Even after inclusion of the thresholds, the formulas overestimate microscopic results by a factor of 10. We note, that both these transition modes are induced by a hole degree of freedom. It suggests, that the single-particle density for holes is much lower than the one for particles. Actually, it is confirmed by the analysis of the single particle states below and above the Fermi level. Accordingly, we differentiated g for particle and hole degrees of freedom in Eqs. (19), (20), and (21). Choosing $g_p/g_h = 3$ and increasing g_p by 20% over the standard value of N (or Z)/13 the dashed-dotted lines in Figs. 6 and 7 are obtained. Such a choice clearly leads to

the improved description of the hole induced transitions, without destroying previous agreement for the remaining ones. In a future paper we plan to address the problem of single particle state densities for particles and holes in more detail.

In Table II we list the accessible state densities for pair creation transitions [for the decay of (1011) configurations in ^{90}Zr at excitation energy 18 MeV] calculated in different approximations. Transition densities were summed over appropriate diagrams to allow for the comparison with the one component model predictions. The most striking result of this comparison is a factor of 10 by which one-component formula with $g = A/13$ overestimates the microscopically calculated value. Us-

ing the two-component formula [Eq. (19)], with $g_p = g_h$ and configuration thresholds set to 0, this factor is roughly reduced to 4. The reduction is understood as being due to the elimination of the spurious transitions in the two-component model (see Ref. 9). Accounting for the configuration thresholds and for the difference between g_p and g_h each decreases transition densities by $\frac{1}{2}$, that results in a fair agreement with the microscopic calculations. Strong reduction of the accessible state densities should lead to the more reasonable mean free path in the exciton model, which used to be unphysically long.

CONCLUSIONS

The reformulation of the two-component exciton model presented in this paper consists in the introduction of the microscopically calculated densities of quasiparticle states, and of the transformation of the master equation to a form in which it can be easily solved using standard numerical methods. To calculate all transition rates for the first three stages of the equilibration chain in the

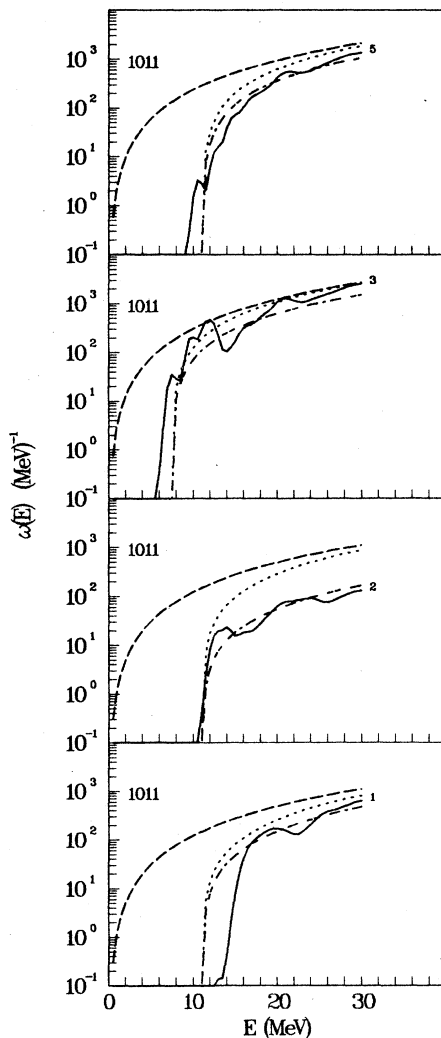


FIG. 6. Comparison of the microscopically calculated accessible state densities (solid lines) with the predictions of the closed formulas [Eqs. (19), (20), and (21)]. The latter are given for $T_i = 0$, $g_p = g_h$ (dashed lines), for $T_i \neq 0$, $g_p = g_h$ (dotted lines), and for $T_i \neq 0$, $g_p \neq g_h$ (dashed-dotted lines). Results correspond to the decay of (1011) substage in ^{90}Zr , and particular transition densities are labeled with the number of the diagram (Fig. 4) to which they correspond.

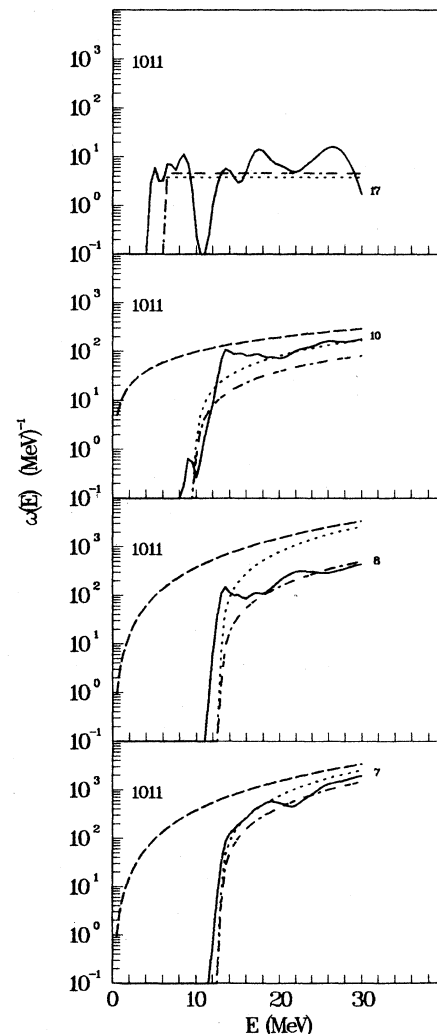


FIG. 7. The same as Fig. 6.

TABLE II. Influence of spurious transitions, configuration thresholds, and g on forward transition densities for (1011) configurations in ^{90}Zr at excitation energy of 18 MeV.

	Shell-model	Eq. (19) $g_p \neq g_h$ $T_i \neq 0$	Eq. (19) $g_p = g_h$ $T_i \neq 0$	Eq. (19) $g_p = g_h$ $T_i = 0$	One-component formula ^a
ω^{++}	672	622	1212	2217	
$\omega^{+\varrho}$	803	639	1455	2771	
ω^+	1475	1261	2667	4988	13 439

$$^a \omega^+(E, n) = g^3 E^2 / 2(n+1); g = \frac{90}{13}$$

frame of the shell model, one only needs several seconds on IBM-3090 computer (without using vector facility). We may thus conclude, that the two-component exciton model calculations using microscopic state densities are feasible, also for the routine applications.

Analyzing transition rates for the decay of the initial stages of the composite nucleus we have shown that, due to the shell structure, a nonuniform flow of the flux through different substages is expected.

It has been found that the leading decay mode is the creation of the particle-hole pair of a given nucleon type by a particle of the opposite nucleon type (unlike-type interaction). This implies that a system, during its equilibration, will tend to populate mostly substages with not too different number of neutron- and proton-type excitons. In addition, it turned out that transitions induced by the holes are strongly suppressed, due to the low density of the the single-particle states below the Fermi energy. The latter, decreasing dependence of the exciton model on the hole interaction, should facilitate the possible experimental verification of the assumptions underlying the exciton and Hybrid models (strong configuration mixing versus no configuration mixing), as proposed recently by Bisplinghoff.²²

The reformulated two-component exciton model, by allowing for the microscopic few-quasiparticle state densities, provides a tool for the theoretical investigation of the structure in the particle spectra observed in several experiments.²⁵⁻²⁸ Interpretation of the structure in the particle spectra emitted from the preequilibrium stages of the composite nucleus may shed some light on the role of the configuration mixing in few quasiparticle states. We consider this an important point, since constraints put by the averaged spectra and the structureless angular distributions, that were analyzed so far, seem to us insufficient to discriminate between various approaches. Such an analysis hopefully may give additional information about the validity of the various preequilibrium models by opening to interpretation a qualitatively new type of the experimental data already available.

ACKNOWLEDGMENTS

The authors wish to acknowledge extensive and fruitful discussion with J. Bisplinghoff. This work has been supported in part by Ente Nazionale Energie Alternative Contract Nos. 6886 and 25888, and under IAEA Contract No. 4644/R1/CF.

¹E. Běták, and J. Dobeš, *Acta. Phys. Slov.* **29**, 76 (1979).

²E. Běták, P. Obložinský, and I. Ribanský, *Nukleonika* **19**, 687 (1974).

³J. Dobeš, and E. Běták, *Z. Phys. A* **310**, 329 (1983).

⁴C. Kalbach, *Phys. Rev. C* **33**, 818 (1986).

⁵C. Birattari, E. Gadioli, E. Gadioli Erba, A. M. Grassi Strini, G. Strini, and G. Togliaferrì, *Nucl. Phys. A* **201**, 579 (1973).

⁶C. Kalbach-Cline, *Nucl. Phys. A* **193**, 417 (1972).

⁷C. Kalbach, *Z. Phys. A* **283**, 401 (1977).

⁸M. Herman, A. Marcinkowski, and K. Stankiewicz, *Nucl. Phys. A* **430**, 69 (1984).

⁹S. K. Gupta, *Z. Phys. A* **303**, 329 (1981).

¹⁰T. Ericson, *Adv. Phys.* **9**, 425 (1960).

¹¹F. C. Williams, *Nucl. Phys. A* **166**, 231 (1971).

¹²C. Costa, Ph.D. thesis, University of Bologna, 1981; G. Reffo, C. Costa, F. Fabbri, in *Proceedings of the International Conference on Nuclear Physics, Florence, 1983*, edited by P. Blasi and R. A. Ricci (Tipografia Compositori, Bologna, 1983).

¹³H. Gruppelaar, C. Costa, D. Nierop, and J. M. Akkermans, *Proceedings of the International Conference on Nuclear Data for Science and Technology, Antwerp Sept. 1982*, edited by K. H. Boeckhoff (Reidel, Dordrecht, 1983), p. 537.

¹⁴H. Gruppelaar, *Proceedings of the IAEA Advisory Group Meeting on Basic and Applied Problems of Nuclear Level Densities*, New York, 1983, Brookhaven National Laboratory Report No. BNL-NCS-51694, 143, 1983 (unpublished).

¹⁵M. Herman and G. Reffo, *Phys. Rev. C* **36**, 1546 (1987).

¹⁶M. Herman, G. Reffo, and R. A. Rego, *Phys. Rev. C* **37**, 797 (1988).

¹⁷J. R. Nix and P. Möller (private communication).

¹⁸F. J. Luider, *Z. Phys. A* **284**, 187 (1978).

¹⁹Essentially, it is not true for the first stage of the reaction, for which no emission is normally assumed. Formally, this difficulty may be overcome by allowing for an arbitrary small emission from the first stage, which would contribute to the elastic channel, without affecting the final result.

²⁰J. H. Wilkinson, *The Algebraic Eigenvalue Problem*, 1st edition (Clarendon, Oxford, 1965), p. 71 and pp. 335-337.

²¹F. J. Luider, ECN Report 17, Netherlands Energy Research Foundation, Petten N. H., 1977 (unpublished).

²²J. Bisplinghoff, *Phys. Rev. C* **33**, 1569 (1986).

²³C. Y. Fu, *Nucl. Sci. Eng.* **86**, 344 (1984).

²⁴F. C. Williams, Jr., *Phys. Lett.* **31B**, 184 (1970).

²⁵W. Scobel, M. Blann, T. T. Komoto, M. Trabandt, S. M. Grimes, L. F. Hansen, C. Wong, and B. A. Pohl, *Phys. Rev.*

- C 30, 1480 (1984).
- ²⁶M. Blann, S. M. Grimes, L. F. Hansen, T. T. Komoto, B. A. Pohl, W. Scobel, M. Trabandt, and C. Wong, Phys. Rev. C 32, 411 (1985).
- ²⁷K. Harder, A. Kaminsky, E. Mordhorst, W. Scobel, and M. Trabandt, Phys. Rev. C 36, 834 (1987).
- ²⁸Y. Wantanabe, I. Kumabe, M. Hyakutake, N. Koori, K. Ogawa, K. Orito, K. Akagi, and N. Oda, Phys. Rev. C 36, 1325 (1987).